14th European Signal Processing Conference (EUSIPCO 2006), Florence, Italy, September 4-8, 2006, copyright by EURASIP

STEREO-POLARIMETRIC MEASUREMENT OF PAIR OF MUELLER IMAGES FOR THREE DIMENSIONAL PARTIAL RECONSTRUCTION

Jawad Elsayed Ahmad and Yoshitate Takakura

Université Louis Pasteur,
Laboratoire des Sciences de l'Image et de la Télédétection, CNRS UMR 7005,
Bld Sébastien Brant, 67412 Illkirch, France.
phone: + (33) 0390244529, fax: + (33) 0390244531, email: jawadsayed@termxjy.u-strasbg.fr

ABSTRACT

Stereoscopy is well adapted for performing three dimensional partial reconstruction. Classical stereoscopy uses conventional scalar images for representing three dimensional objects. Thus all the necessary tasks (segmentation, classification, edge detection, correspondence matching) are performed on the classical scalar images. For some particular cases like improperly illuminated scenes, camera blindness by a bright edge response and for transparent objects detection, scalar images do not provide us with the reliable foundation from which precise three dimensional partial reconstruction can be performed (bad segmentation, hidden contour, undetected region, false classification). The object of this paper is to show how, very simply, by controlling the polarization state of the imaging system we can overcome the above mentioned problems. On the conceptual level, the contribution of polarimetry to the stereoscopy will be highlighted by a quantitative analysis of the precision of three-dimensional reconstruction of objects.

1. INTRODUCTION

In classical stereoscopic image acquisition for three dimensional partial reconstruction used in industrial objects application and quality control we always encounter difficulties with the light sources positioning. The bad positioning of these light sources can directly affect the image quality of the object (low contrast level, undetected contours, bright edge response, camera blindness) and thus it will enormously affect the three dimensional reconstruction precision. These problems are usually treated by changing the position of the light sources and thus we may have for each object under investigation specific light sources positioning which is delicately not practical and time consuming. A good approach to automatically test the quality of the image is by testing the histogram distribution of the intensity values. If the histogram graph contains high peaks on one of its extremities we say that we are encountered with an ill-illuminated image and we must modify the light position and illumination. In addition to that, having for example a given scene with multiple source positions and we have encountered problems in detecting an edge so we have planed to make some changes in the light positioning to try to appear the badly illuminated region or this undetected edge, it is not obvious to know which light source position we must modify and in which direction. In active optical imagery, having the possibility of modifying the polarization of the illumination source and of the analyzing system makes it possible to reveal transparent and hidden contours and to attenuate the intensity coming from bright edges, without changing the light source position, thanks in particular to the Fresnel response of the interfaces, coupled by the diffusion related to the surface inhomogeneities, see Fig.1. Such a method, the polarimetric imagery, naturally represents a solution for the physical constraints to which are subjected the conventional stereoscopy.

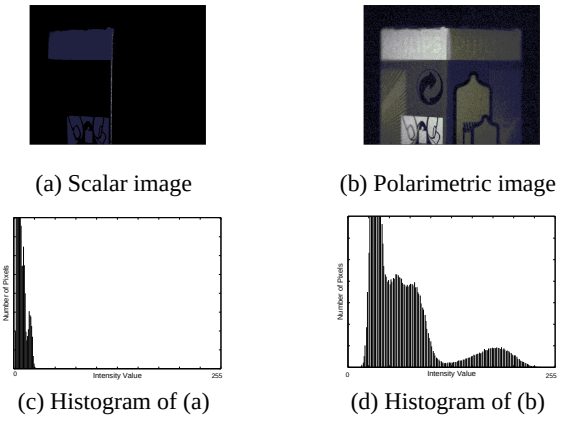

(a) Scalar image (b) Polarimetric image

(c) Histogram of (a) (d) Histogram of (b)

Figure 1: (a) Camera blindness by a bright edge response, (b) eliminating the edge response effect by changing the polarization state of the incident and analyzing systems, (c) histogram of the poorly illuminated object, (d) by changing the polarization state we have managed to obtain a satisfactory histogram distribution.

2. MUELLER IMAGE

The astonishing accurate dependence between the polarimetric information extracted from a given object and its material properties and shape still the point of admiration of many scientists working in the branch of polarimetry. we define polarimetry as the sciences of measuring the polarization state of light which can be characterized by four real intensity parameters called the Stokes parameters usually expressed as four dimensional column vector called the Stokes vector, $\mathbf{S} = [S_0, S_1, S_2, S_3]^T$. The general transformation between the incident Stokes vector $\mathbf{S_{in}}$ and the emergent Stokes vector $\mathbf{S_e}$ resulting from a linear interaction with an optical system or a sample can be described by a 4×4 real matrix $\mathbf{M}$ called the Mueller matrix.

$$\mathbf{S_{in}} = \mathbf{M} \cdot \mathbf{S_e} \tag{1}$$

Mueller calculus can be applied to incoherent states, it can describe polarized, partially polarized, or unpolarized light

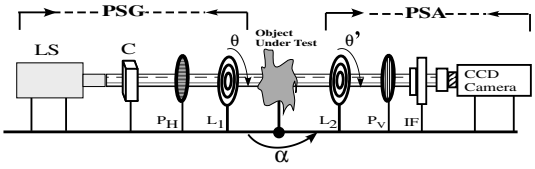

Figure 2: Experimental system setup. LS: incoherent light source, C: collimator, $P_{H,V}$: horizontal and vertical linear polarizers, $L_{1,2}$: rotating quarter wave plates, θ, θ': angle of rotation with respect to the fast axis, IF: interferential filter centered at $\lambda = 632.8$ nm, α: view angle position of the **PSA**.

and can quantify depolarization. We define Mueller matrix image as two-dimensional measurements of the Mueller matrix attached to each pixel. Such image can reveal contrasts between two different zones that have the same intensity reflectivity. The latter point has encouraged us to benefit from the Mueller image when making stereoscopic reconstruction of three dimensional objects because the Mueller image is more adapted to overcome problems of the ill-illumination conditions of the scene and can detect transparent objects while conventional images fail to accomplish these tasks, see Fig.3.

2.1 Experimental setup

In our laboratory we are using a classical active Stokes-Mueller imaging polarimeter [1], made up from an incoherent light source, two linear polarizer (P_H, P_V), two quarter wave plates (L_1, L_2) and an interferential filter followed by a CCD camera, Fig. 2. The polarization state generator, **PSG**, can generate different polarization states by rotating, with an angle θ, its input quarter wave plate (L_1) fast axis with respect to the reference vertical axis. On the other side, the polarization state analyzer **PSA** furnish us changing analyzer basis by which we will be capable to analyze any impinging wave. The received intensity upon the CCD camera is formed from a linear combination between the **PSG**, the object under test characterized by its Mueller matrix and the **PSA**, it takes the following form,

$$\mathbf{I}(\theta_1 \cdots \theta_k, \theta'_1 \cdots \theta'_l) = \mathbf{A}_{l\times 4} \cdot \mathbf{M}_{4\times 4} \cdot \mathbf{G}_{4\times k} \qquad (2)$$

where **G** and **A** are the **PSG** and the **PSA** matrices respectively and k, l are the numbers of angle positions θ, θ' that have made the two quarter wave plates $L1$, $L2$ with respect to the vertical axis during the whole measuring process. Presetting our matrices **A**, **G** and measuring the scattered intensity upon the CCD camera we can obtain the Mueller image for an object under test by inverting Eq.(2) for each pixel and applying the following inversion,

$$\mathbf{M}_{4\times 4} = \mathbf{A}^{\sharp}_{4\times l} \cdot \mathbf{I}_{l\times k} \cdot \mathbf{G}^{\sharp}_{k\times 4} \qquad (3)$$

The superscript $\sharp$ denotes the matrix Pseudo-inverse. The only condition for Eq.(3) to be realizable is that the matrices **A**, **G** are invertible, thus $(k, l) \geq 4$.

3. STEREO-POLARIMETRIC IMAGE PROCESSING

For stereo-polarimetric three dimensional partial object reconstruction a well convenient structure is illustrated in Fig.4. We must keep in mind that we are working with physical polarimetric images, this explains the presence of the physical realizability test, see section 3.3. This test constitute a necessary step when treating any polarimetric image.

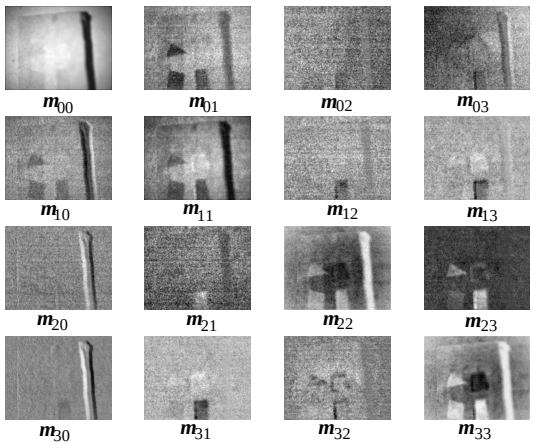

Figure 3: Mueller image of four geometric objects. m_{00} is the intensity image. In image m_{33} we have identified a transparent square that was impossible to be detected within the intensity image.

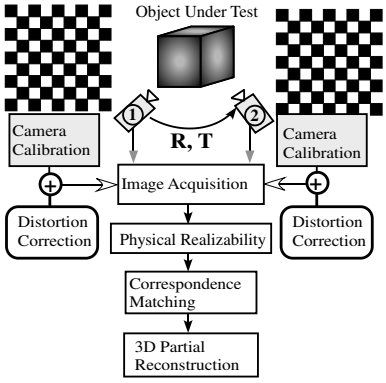

Figure 4: Stereo-polarimetric structure for three dimensional partial reconstruction.

3.1 The epipolar geometry

Two images of a single scene are called stereoscopic images. Using the pinhole camera model [2], stereoscopic images can be related by a geometrical coplanarity constraint called the epipolar constraint. The epipolar geometry can be expressed mathematically by a 3×3 singular matrix (**F**) called the fundamental matrix [3]. The matrix **F** allows us to reduce the correspondence search area, for every pixel m in image1, to a single line lying on image2 called the epipolar line rather than searching all the pixels in image2. In Fig.5, the points M, m, m',C_1, C_2, e and e' lie in the same plane called the epipolar plane. For every point correspondence $m_i = [u_i, v_i, 1]^T$ and $m'_i = [u'_i, v'_i, 1]^T$ we can write,

$$m_i'^T \mathbf{F}_{12}\, m_i = 0 \qquad (4)$$

The fundamental matrix **F** can thus be determined up to a scale factor using 8 point matches satisfying Eq.(4).

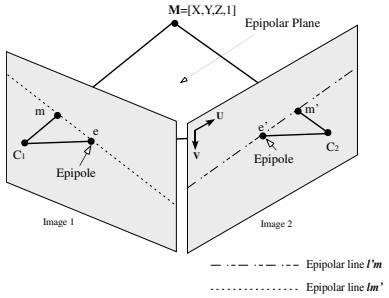

Figure 5: Stereoscopic images are related by the epipolar geometry. M: 3D point in the space. U,V: image coordinate system. C_1,C_2: camera focal point. e,e': epipoles. m and m' are two corresponding points. m' lies on the epipolar line $l'm$ that arises from the projection of the line C_1M on image2.

Knowing the camera intrinsic parameters (focal length, optical center, ...) and the rigid displacement between the two optical centers, C_1 and C_2, we can also determine the fundamental matrix by geometrical calculation $\mathbf{Fg}_{12}$ as,

$$\mathbf{Fg}_{12} = \mathbf{A}_2^{-T}\mathbf{TRA}_1^{-1} \tag{5}$$

where $\mathbf{A}_{1,2}$ are the camera intrinsic matrices, defined in section 3.2, for camera1 and camera2 respectively, $\mathbf{T}$ is an antisymmetric matrix characterizing the translation between the two optical centers and $\mathbf{R}$ is the 3D Euler's rotation matrix between the two cameras coordinates axis.

3.2 Camera calibration and distortions correction

We have carried out the calibration procedure based on a planar square rig shown in Fig.4, the formalism proposed in [4, 5] was used to calculate the planar homographies between images. After that, the camera intrinsic parameters can be extracted by having at least two images of the square rig taken with different orientations (Rotation+Translation).
The estimation of the distortion parameters was performed separately from the camera calibration using the single view technique described in [6, 7]. In this technique we take images for purely straight lines and we calculate the deviation of the images line from the reality. This small deviation can be then modeled as distortion parameters.

3.3 Physical realizability of the Mueller image

When applying Eq.(3) on each pixel of the captured intensity images we risk to obtain some pixels that are not physically significant because not every 4×4 real matrix is a physical Mueller matrix. A physical Mueller matrix is a matrix that, for all the incident physical Stokes vector ($\mathbf{S_{in}}$), the output of Equation (1) is always a physical Stokes vector ($\mathbf{S_e}$). A method to test the physical realizability of a Mueller matrix is to test the Degree of Polarization, $\mathbf{DoP}$, of the output Stokes vector for all the physical combinations of an incident Stokes vector lying on the Poincaré sphere,

$$\mathbf{DoP} = \frac{I_{polarized}}{I_{total}} = \frac{\sqrt{\mathbf{S_{e1}}^2+\mathbf{S_{e2}}^2+\mathbf{S_{e3}}^2}}{\mathbf{S_{e0}}} \tag{6}$$

For a physical Mueller matrix the conditions on $\mathbf{S_e}$ are: $0 \le \mathbf{DoP} \le 1$, $\mathbf{S_{e0}} > 0$ and $\mathbf{S_{e0}} \le \mathbf{S_{in0}}$. For totaly polarized light, $\mathbf{DoP} = 1$. The distribution undertaken by all the points lying on the Poincaré sphere can be visualized within a surface map of the Degree of Polarization. In Fig.6 we notice the effect of a given Mueller matrix on the Poincaré sphere. The points of contraction and extraction on the map defines the diattenuation axis of the Mueller matrix.

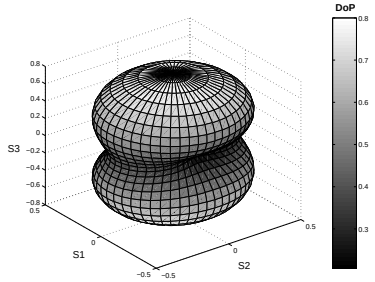

Figure 6: Degree of polarization surface plot for a non uniform depolarizing Mueller matrix.

3.4 Correspondence matching

After restricting the correspondence search area over the epipolar line, which is a direct consequence from the coplanarity constraint, we must find the exact pixel m'_i in image2 lying on the epipolar line $l'_i m_i$ that corresponds to the point m_i in image1.
The method consists of calculating the fundamental matrix by both ways using Eq.(4) to calculate $\mathbf{F}_{12}$ and by exactly controlling the rigid motion from C_1 to C_2 we can calculate $\mathbf{Fg}_{12}$ as in Eq.(5). In our laboratory we have a horizontal displacement between the two cameras, so the $\mathbf{Fg}_{12}$ fundamental matrix will always produce horizontal epipolar lines. On the other hand $\mathbf{F}_{12}$ was calculated using the normalized eight point algorithm [8] from different point matches followed by a nonlinear minimization of the Sampson distance [9].
The pixel by pixel correspondence matching technique consists of searching, for a given point m in image1, for the intersection point between the two epipolar lines arising from the two different methods of calculating the fundamental matrix. The intersection point m' in image2 of these two epipolar lines is the match point of m, Fig. 7.

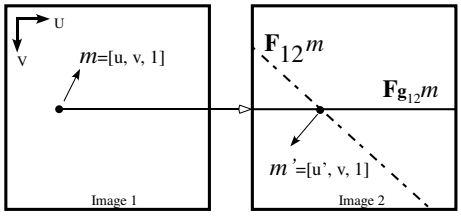

Figure 7: Pixel by pixel matching technique. The point m' is obtained from the intersection of the two epipolar lines.

3.5 Three dimensional reconstruction

In this section we present experimental results made on a simple object where we have resolved the problem caused by a bright edge response by means of polarimetric treatments. Firstly, we have recorded the measured intensity images from the CCD camera for the object at angle $\alpha = \alpha_1$,

then the Mueller image was calculated using Eq.(3). The same thing is done but after changing the **PSA** view angle to $\alpha = \alpha_2$, hence we have managed to form a set of stereo-polarimetric images. Secondly, after performing an image

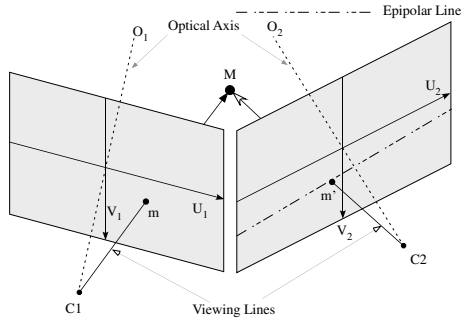

Figure 8: Performing 3D reconstruction by triangulation from two image correspondence.$C_{1,2}$: Camera optical center. $O_{1,2}$: Optical axis. m, m': Two matching points. **M** is the reconstructed 3D position.

segmentation we have searched for point correspondence to calculate the normalized fundamental matrix $\mathbf{F}_{12}$. Then by previously knowing the matrix $\mathbf{Fg}_{12}$ we can manage to represent the three dimensional position of any point match as described in section 3.4. For time consuming purpose, we have triangulate our left image and then searched for the corresponding point to the triangles vertices only. From the vertices correspondence we can build the 3D triangles representation of the object. When performing three dimensional reconstruction for each vertex match the pinhole camera model was adopted and it is defined, for the first and second position respectively, by its optical center position $C_{1,2}$, its optical axis $O_{1,2}$ and its image plane called the retinal plane determined by the two perpendicular vectors $U_{1,2}$ and $V_{1,2}$ [10]. The point **M** is the intersection of the two viewing lines C_1m and C_2m'. If the viewing lines do not intersect the spatial position **M** is assumed to be located at the point with minimal distance to both viewing lines, Fig.8. Finally, we have managed to texture each 3D reconstructed triangle by its original texture by patching the image triangles into the three dimensional reconstructed triangles.

In Fig.9 we present the results performed on an industrial object under test where we have profited from the polarimetry to solve the bright edge response problem that was blinding the camera. Unfortunately this object does not contains any transparent area, thus we could not totaly exploit the power of the Mueller image for the reconstruction of transparent objects.

4. CONCLUSION

In this paper we have pointed out to the Mueller image richness that can be suitable in eliminating all the problems posed by the light sources illumination control, also in the detection of transparent objects, Fig.3. Thus the possibility to extract the physical response from the object/scene under test. In addition to illumination control problem solving, we can extend our results to carry out the stereo-polarimetric reconstruction technique for biological cells and exactly to detect, by the Mueller image, the presence of contaminated cells within certain region of interest that will have different polarimetric

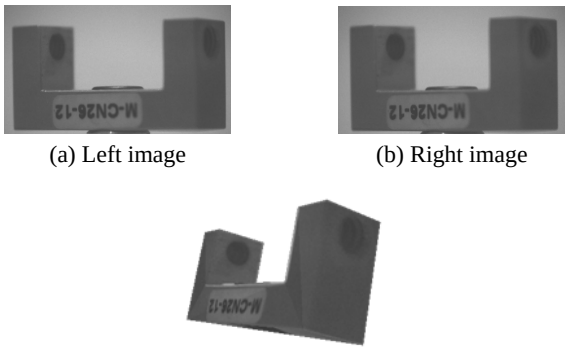

(a) Left image (b) Right image

(c) 3D Reconstructed object

Figure 9: Three dimensional partial representation of an industrial object using stereo-polarimetric images.

response than normal cells. Then to use the stereovision to locate the three dimensional positions of these cells.

REFERENCES

[1] J.L. Pezzaniti, R.A. Chipman, "Mueller matrix imaging polarimetry", Opt. Eng., vol. 34, pp.1558-1568, 1995.

[2] Z. Zhang, "Determining the fundamental matrix and its uncertainty", INRIA Report No. 2927, 1996.

[3] B. Albouy, S. Treuillet, Y. Lucas, D. Birov, "Fundamental matrix estimation revisited through a global 3D reconstruction framework", *Advanced concepts for intelligent vision systems*, pp.185-192, 2004.

[4] Z. Zhang, "A Flexible New Technique for Camera Calibration", Technical Report MSR-TR-98-71, Microsoft Research, 1998.

[5] J. Heikkilä, O. Silvén, "A Four-step Camera Calibration Procedure with Implicit Image Correction", Proc. CVPR'97, *IEEE*, pp.1106-1112, 1997.

[6] F. Devernay, O. Faugeras, "Automatic calibration and removal of distortion from scenes of structured environments", *SPIE*, vol. 2567, 1995.

[7] T. Thormählen, H. Broszio, I. Wassermann, "Robust Line-Based Calibration of Lens Distortion from a Single View", *Mirage 2003*, pp.105-112, 2003.

[8] R. Hartley, "In the defense of the Eight point Algorithm", *IEEE transaction on pattern analysis and machine intelligence*, vol. 19, No. 6, 580-593, 1997.

[9] R. Hartley, A. Zisserman, *Multiple View Geometry*, Cambridge university press, UK, 2000.

[10] R. Koch, "Model-Based 3D scene Analysis from stereoscopic Image sequences", Proc. Int. Soc. Photogram. Remote Sens., Washington, DC, 1992.